Recommendation ITU-R P.1410-6

(08/2023)

P Series: Radiowave propagation

Propagation data and prediction methods required for the design of terrestrial broadband radio access systems operating in a frequency range from 3 GHz to 60 GHz

Foreword

The role of the Radiocommunication Sector is to ensure the rational, equitable, efficient and economical use of the radio-frequency spectrum by all radiocommunication services, including satellite services, and carry out studies without limit of frequency range on the basis of which Recommendations are adopted.

The regulatory and policy functions of the Radiocommunication Sector are performed by World and Regional Radiocommunication Conferences and Radiocommunication Assemblies supported by Study Groups.

Policy on Intellectual Property Right (IPR)

ITU-R policy on IPR is described in the Common Patent Policy for ITU-T/ITU-R/ISO/IEC referenced in Resolution ITU-R 1. Forms to be used for the submission of patent statements and licensing declarations by patent holders are available from http://www.itu.int/ITU-R/go/patents/en where the Guidelines for Implementation of the Common Patent Policy for ITU-T/ITU-R/ISO/IEC and the ITU-R patent information database can also be found.

<table>
<tr><td colspan="2" align="center">**Series of ITU-R Recommendations**</td></tr>
<tr><td colspan="2" align="center">(Also available online at https://www.itu.int/publ/R-REC/en)</td></tr>
<tr><td>**Series**</td><td align="center">**Title**</td></tr>
<tr><td>**BO**</td><td>Satellite delivery</td></tr>
<tr><td>**BR**</td><td>Recording for production, archival and play-out; film for television</td></tr>
<tr><td>**BS**</td><td>Broadcasting service (sound)</td></tr>
<tr><td>**BT**</td><td>Broadcasting service (television)</td></tr>
<tr><td>**F**</td><td>Fixed service</td></tr>
<tr><td>**M**</td><td>Mobile, radiodetermination, amateur and related satellite services</td></tr>
<tr><td>**P**</td><td>**Radiowave propagation**</td></tr>
<tr><td>**RA**</td><td>Radio astronomy</td></tr>
<tr><td>**RS**</td><td>Remote sensing systems</td></tr>
<tr><td>**S**</td><td>Fixed-satellite service</td></tr>
<tr><td>**SA**</td><td>Space applications and meteorology</td></tr>
<tr><td>**SF**</td><td>Frequency sharing and coordination between fixed-satellite and fixed service systems</td></tr>
<tr><td>**SM**</td><td>Spectrum management</td></tr>
<tr><td>**SNG**</td><td>Satellite news gathering</td></tr>
<tr><td>**TF**</td><td>Time signals and frequency standards emissions</td></tr>
<tr><td>**V**</td><td>Vocabulary and related subjects</td></tr>
</table>

Note: *This ITU-R Recommendation was approved in English under the procedure detailed in Resolution ITU-R 1.*

Electronic Publication
Geneva, 2023

© ITU 2023

RECOMMENDATION ITU-R P.1410-6

Propagation data and prediction methods required for the design of terrestrial broadband radio access systems operating in a frequency range from 3 GHz to 60 GHz

(Question ITU-R 203/3)

(1999-2001-2003-2005-2007-2012-2023)

Scope

Broadband wireless access is an important method of providing broadband to individual households as well as small business enterprises. This Recommendation addresses systems in a frequency range from 3 to 60 GHz and gives guidance for line-of-sight (LoS) coverage and non-LoS propagation mechanisms of importance. For affected systems, rain methods are given to estimate diversity improvement by selecting the best base station from two and the coverage reduction under rainfall. Guidance is given regarding wideband distortion.

Abbreviations/Glossary

BS	Base station
BWA	Broadband wireless access
C/*I*	Carrier to interference ratio
CIR	Carrier power to interference power ratio
DVB-S	Satellite digital video broadcasting
FEC	Forward error correction
HiperMAN	High performance radio Metropolitan Area Network
LMCS	Local multipoint communications system
LMDS	Local multipoint distribution system
LoS	Line of sight
MPC	Maximum power combiner
MPEG-2	Moving pictures experts group-2
non-LoS	non-line of sight
pfd	power flux-density
P-MP	Point-to-multipoint
QPSK	Quadrature phase shift keying
SAR	Synthetic aperture radar
SS	Subscriber station

Related ITU Recommendations, Reports

Recommendation ITU-R P.1411

Recommendation ITU-R P.833

Recommendation ITU-R P.526

Recommendation ITU-R P.452

Recommendation ITU-R P.530

Recommendation ITU-R P.1057

NOTE – The latest revision/edition of the Recommendation/Report should be used.

The ITU Radiocommunication Assembly,

considering

a)   that for proper planning of terrestrial broadband radio access systems it is necessary to have appropriate propagation information and prediction methods;

b)   that Recommendations established for the design of individual links do not cover area aspects,

recommends

that the propagation information and prediction methods set out in Annex 1 should be used when designing terrestrial broadband radio access systems, operating in a frequency range from 3 GHz to 60 GHz.

Annex 1

TABLE OF CONTENTS

1 Introduction

There is a growing interest in delivery of broadband services through local access networks to individual households as well as small business enterprises. Radio solutions are being increasingly considered as delivery systems, and these are now available on the market. Several systems are being considered and introduced, such as local multipoint distribution system (LMDS), local multipoint communications system (LMCS), and point-to-multipoint (P-MP) system. Collectively, these systems may be termed broadband wireless access (BWA). International standards are being developed, for example WMAX based on IEEE 802.16 and HiperMAN.

There is a need within the network planning, operator, and manufacturing communities and by regulators for good design guidance with respect to radiowave propagation issues.

2 Area coverage

When a cellular system is planned the operator has to carefully select base station location and height above the ground to be able to provide service to the target number of users within an area. The size of the cells may vary depending on the topography as well as on the number of users for which the radio service is being offered. This section presents a statistical model for building blockage based on very simple characterization of buildings in an area and provides guidance based on detailed calculations. It also presents a vegetation attenuation model and some simple design rules.

2.1 Building blockage

Building blockage probability is best estimated by ray-tracing techniques using real data from detailed building and terrain databases. The requirements for ray-tracing techniques are briefly described in § 2.1.1. However, in many areas, suitable databases are not available, and the statistical model outlined in § 2.1.2 is recommended.

2.1.1 Ray-tracing requirements

An accurate coverage prediction can be achieved using ray-trace techniques in areas where a database of land coverage is available. Owing to the high frequency and short path lengths involved, straight line geometric optical approximations can be made.

To a first order of approximation in estimating coverage, an optical line-of-sight (LoS) determination of 60% of the 1st Fresnel zone clearance is sufficient to ensure negligible additional loss (see Fig. 1). Diffraction loss for non-LoS cases is severe. The accuracy of the buildings database will limit the accuracy of the ray prediction and the database must include an accurate representation of the terrain and buildings along the path. The Earth' curvature must also be considered for paths > 2 km. Buildings and vegetation should be considered as opaque for this procedure.

FIGURE 1

Each building must lie below the LoS ray joining Tx and Rx

P.1410-01
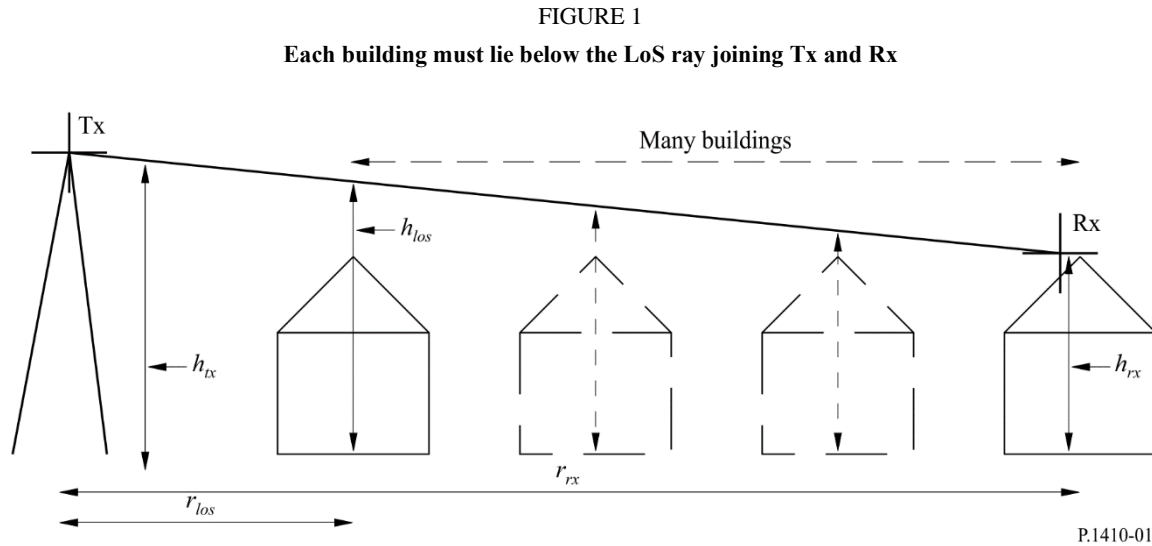
Measurements of signal characteristics when compared against ray-trace models have shown good statistical agreement, but the measurements demonstrated considerable signal variability with position and with time for paths without a clear LoS. Therefore, owing to the limited accuracy of real building databases, predictions of service quality for specific near LoS paths will not be possible.

Vegetation, in particular tall trees and shrubs can cause severe service impairment and vegetation data should ideally be included in the database.

Measurements have indicated that, for service provision in a typical urban/suburban region, users impaired by multipath reflection effects are much rarer than those blocked by buildings or vegetation, owing to the narrow antenna beamwidth, and it is therefore not necessary to calculate reflections (see § 4.2.1).

The database used for ray-tracing evaluation may be a detailed object-oriented database, with terrain height, individual building outlines including roof height and shape data and with vegetation represented as individual trees or blocks of trees. As an alternative, in determining LoS, a raster database of spot height, such as generated from an airborne synthetic aperture radar (SAR) measurement may be used (see Table 1).

TABLE 1

Minimum database requirements

Object	Format	Horizontal resolution (m)	Vertical resolution (m)
Terrain	Grid of spot heights	50	1
Buildings	Object oriented or high resolution raster image	1	1
Vegetation			

2.1.2 Dealing with reflections and scattering

In an urban environment, reflections off nearby buildings can be the dominant propagation mechanism in non-LoS conditions. Efficient methods to calculate reflections in large databases have been the subject of much research and literature. When considering multiple reflections and diffractions the problem becomes intractable for all but the most trivial of scenarios. For this reason

a single-bounce reflection model, with each path to and from the reflector being subject to its own vertical and horizontal diffractions losses is recommended.

The rough surface scatter model

It is suggested that to minimize computational overhead the simple model given here be used. The model is a scalar model for the incoherent scatter from a rough surface. That is, it only considers scattered power and ignores phase and polarization effects.

Geometry

Consider a rough surface facet F of area A. Let T and R be a transmitter and receiver. $\vec{i}$ and $\vec{m}$ are unit vectors in the directions TF and FR and n is the normal to the facet, Fig. 2.

FIGURE 2

Reflection geometry
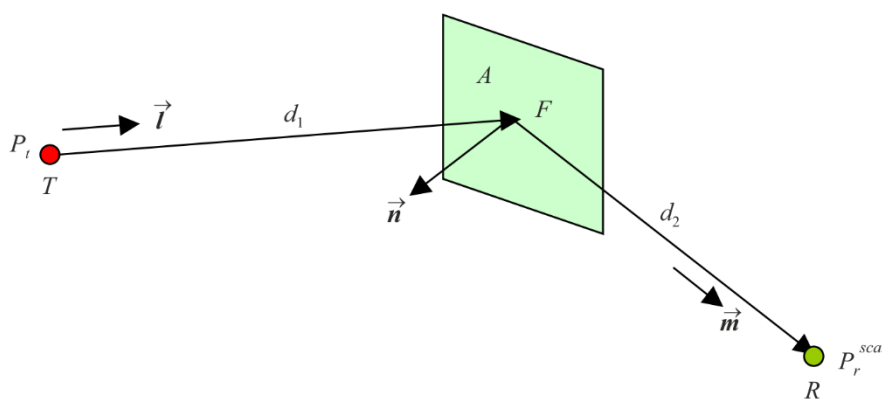
P.1410-02

P_t and P_r^{scat} are the transmitted and received, scatter powers at T and R respectively and, without loss of generality, we assume omnidirectional antennas at T and R.

Propagation from T to F

Assuming free-space propagation, the power flux-density (pfd) S (W/m^2) at distance d_1 from T is:

$$S = \frac{4\pi}{\lambda^2}\left(\frac{\lambda}{4\pi d_1}\right)^2 P_t \qquad (1)$$

where λ is the wavelength. The power P_{fr} impinging on F is then:

$$P_{fr} = SA\left|\vec{1}\cdot\vec{n}\right| \qquad (2)$$

This result assumes that any dimension of $A \ll d$ so that the pfd is constant across the facet. This is not a strong constraint: in principle the facet A may be taken as small as necessary to make this true. However, in this model it is assumed that F is in fact a whole building face (or at least the illuminated portion of a building face), and it is assumed that this constraint is satisfied. The reference point for the scatter is the centre of the facet.

Model of rough surface scatter

The model is one used for rendering diffuse scatter in computer graphics. It assumes that the incoherent power scattered by the rough surface F is Lambertian. That is, the power is re-radiated in all directions (in the half plane) with an intensity that varies as $\cos \theta$ where θ is the angle of radiation to the normal. This variation exactly cancels the $1/\cos \theta$ dependence of the emitted pfd (due to the $|\vec{\mathbf{m}} \cdot \vec{\mathbf{n}}|$ projection term) giving omnidirectional radiation with equal gain in all directions. This corresponds to what is observed in practice for optical scatter. The incoherent power emitted by F is given by:

$$P_{ft} = 2\rho_{nonspec}P_{fr} \tag{3}$$

The factor 2 accounts for the fact all the power is emitted into a hemisphere. $\rho_{nonspec}$ accounts for the fraction of the coherent power impinging on F that is re-emitted as non-specular scatter.

Propagation from F to R

Assuming free-space propagation and an omnidirectional antenna, the received scatter power at R is:

$$P_r^{scat} = \left(\frac{\lambda}{4\pi d_2}\right)^2 P_{ft} \tag{4}$$

Full link budget

Combining equations (1) and (2) gives:

$$P_r^{scat} = 2\rho_{nonspec}\frac{4\pi A|\vec{\mathbf{I}} \cdot \vec{\mathbf{n}}|}{\lambda^2}\left(\frac{\lambda}{4\pi d_1}\right)^2\left(\frac{\lambda}{4\pi d_2}\right)^2 P_t \tag{5}$$

The $(\lambda/4\pi d)^2$ terms are the free-space propagation terms, and can in general be replaced by the actual propagation terms. Antenna gain patterns at T and R can also be included. The only assumption required is that of plane wave incidence at F.

Scatter loss

It may be useful to calculate the incoherent, rough surface, scatter "loss". This is the additional basic transmission loss incurred by the scatter over and above the basic transmission loss experienced if the facet were a perfect mirror, that is, a specular reflection with a reflection coefficient of 1. To do this we need to assume free-space propagation on paths TF and FR. The received power at R from a transmitter at T under the perfect reflection assumption, P_r^{LoS} is:

$$P_r^{LoS} = \left(\frac{\lambda}{4\pi(d_1 + d_2)}\right)^2 P_t \tag{6}$$

The scatter loss L_{scat} is then (defined so that $L_{scat} > 1$ for a loss):

$$\frac{1}{L_{scat}} = \frac{P_r^{scat}}{P_r^{LoS}} = \frac{|\vec{\mathbf{i}} \cdot \vec{\mathbf{n}}|}{2\pi}\rho_{nonspec}\frac{(d_1 + d_2)^2 A}{d_1^2 d_2^2} \tag{7}$$

All the terms in this expression are strictly < 1 apart from the last term, which can become > 1 if A is too large compared to d_1 and d_2. However as noted above, the model is only valid if any dimension of $A << d_1$ so an implementation of equation (7) should enforce the condition:

$$\frac{(d_1+d_2)^2 A}{d_1^2 d_2^2} \leq 1 \tag{8}$$

This will only be violated for transmitter and receiver positions that are extremely close to F.

Equation (7) shows that the non-specular scatter loss increases rapidly as the reception point moves away from the scatter surface. As $d_1 \to \infty$, the loss (in decibels) $\to 10 \log(d_2^2 / A)$. So for a building face of 100 m² the loss due to this term alone is 20 dB at 100 m and 40 dB at 1 km distance from the building.

Definition of $\rho_{nonspec}$

Defining ρ_{spec} and ρ_{trans} as the fraction of the coherent power impinging on F that is reflected as specular (coherent) reflection and transmitted through the facet, respectively, a consistent model of the complete scatter process might be expected to conserve energy, giving:

$$\rho_{spec} + \rho_{trans} + \rho_{nonspec} = 1 \tag{9}$$

Unfortunately, our semi-empirical model is not consistent, and different assumptions are made for each mechanism:

– ρ_{spec}: the most theoretically based model is that for specular scatter. For a smooth facet, the reflected power is determined by the Fresnel reflection coefficients (which depend on the specular reflection angle, and the electrical properties of the facets). However there is no simple extension for rough surface scattering, and the model uses a semi-empirical term that modifies (reduces) the smooth surface Fresnel reflection coefficient. It is proposed that ρ_{spec} is defined as the power reduction factor due to the rough surface effect alone; that is, it does not take account of reflected power variation due to the Fresnel coefficient variation. The latter depends on the reflection angle and polarization, and therefore so would the non-specular scattered power; this would be incompatible with the Lambertian assumption.

– ρ_{trans}: in principle the transmitted component can also be calculated from Fresnel theory for a smooth surface, single interface. However, in practice, the situation is too complicated to model (rough surface, multiple interfaces and reflections) and an experimentally determined, empirical value for ρ_{trans} should be used.

In principle each ρ must satisfy the condition $0 \leq \rho \leq 1$. There is no reason to believe that equation (9) will be satisfied, and if used to derive $\rho_{nonspec}$ from ρ_{spec} and ρ_{trans}, it is possible for $\rho_{nonspec}$ to become negative which is unphysical. It is proposed therefore that the non-specular fraction is derived directly from the specular fraction, ignoring the transmitted component:

$$\rho_{nonspec} = 1 - \rho_{spec} \tag{10}$$

In practice ρ_{trans} is likely to be quite small (e.g. 10 dB building penetration loss implies $\rho_{trans} = 0.1$).

Calculation of ρ_{spec}

ρ_{spec} is the *power* reduction factor applied to the specular reflection coefficient to account for the effect of surface roughness on specular reflection. It is:

$$\rho_{spec} = \rho_s^2 \qquad (11)$$

When calculating the specular reflection coefficient, the effective reflection coefficient R is obtained by multiplying the Fresnel coefficient R_F by ρ_s:

$$R = \rho_s R_F \qquad (12)$$

ρ_s can be calculated from:

$$\rho_s = \max\left[\exp\left(-\tfrac{1}{2}g^2\right), 0.15\right] \qquad (13)$$

where:

$$g = \frac{4\pi\sigma}{\lambda}\cos\varphi \qquad (14)$$

σ is the standard deviation of the surface roughness height about the local mean within the first Fresnel zone, and φ is the angle of incidence to the surface normal. The 0.15 cut-off in equation (13) is to prevent ρ_s becoming too small. (The exponential term tends to underestimate the scatter for very rough surfaces.)

The calculation of the specular reflection coefficient in equation (13) is complicated. The Fresnel coefficient depends on angle, electrical constants and *polarization*. The dependence on polarization means that, in general, both the parallel and perpendicular Fresnel reflection coefficients need to be calculated, and the ray path geometry needs to take account of polarization rotation when calculating the signal at the receiver.

Given the empirical nature of the model, if the modelling is only concerned with signal powers (and can ignore phase) a simplification may be made through calculating all specular reflections based on only the parallel Fresnel coefficient. The magnitude of the coefficient when the electric vector lies in the plane of the incident and reflected rays (blue or upper curve, in Fig. 3) is always numerically greater than the coefficient when the electric is normal to the plane (in red or lower curve). In a 3-dimensional database, there will generally be a mixing of the two polarization components, and the parallel component will tend to mask out the "null" in the perpendicular component.

Magnitude of the parallel (blue) and perpendicular (red) Fresnel reflection
R_F coefficient as a function of angle (3.5 GHz, medium dry surface)
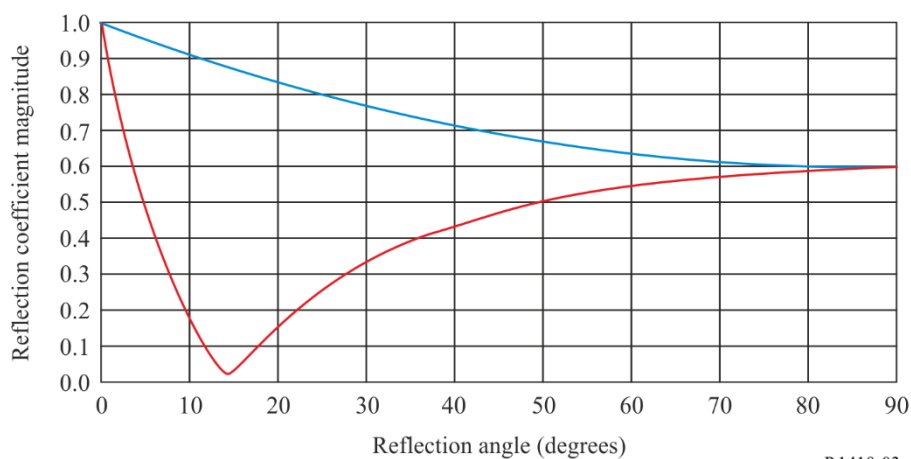
P.1410-03

Calculation of ρ_{trans}

ρ_{trans} is the fraction of the incident power transmitted through the wall. In this application, it is assumed that the value of ρ_{trans} is a constant independent of the transmission angle relative to the facet and that the facet does not change the angle of the ray as it passes through the facet.

Points to note

1 The rough surface scatter loss is given by equation (10) with the non-specular power fraction defined via equations (11), (13) and (14).

2 L_{scat} does not depend explicitly on λ, the only frequency dependence being via ρ_{nonpec}. This is as expected – this is a scalar power model, and the Lambertian source model is independent of frequency.

3 A model that correctly represents phase and polarization would be much more complex and incompatible with an incoherent scatter model. More importantly it would require detailed knowledge of the form of the surface roughness that is never likely to be available. (This might be possible for a "slightly" rough surface, using a perturbation approach, but such a coherent scatter model would be better dealt with within the framework of a modified specular reflection model.)

4 A consequence of point 3 is that this scatter model is really only useful for modelling *interference* since interference powers are assumed to add incoherently. For the wanted signal this result can be used to estimate the delay spread. For the summation needed to get the total signal power, a more detailed consideration of phase (or equivalently, differential path lengths) is necessary.

5 The non-specular scatter model does not satisfy reciprocity. In fact it *almost* does, but the inclusion of the $\left|\vec{\mathbf{l}} \cdot \vec{\mathbf{n}}\right|$ term without a corresponding $\left|\vec{\mathbf{m}} \cdot \vec{\mathbf{n}}\right|$ term destroys the symmetry. By choosing a scatter source model other than Lambertian it could be possible to repair this. However, the model is semi-empirical in any case, and reciprocity is not to be expected with the simple assumptions made.

2.1.3 Transmission through buildings

Measurements reported in Recommendation ITU-R P.1411 and (reported measurements references) show that signal penetration through buildings over the lower end of the frequency range may become

a significant propagation mechanism (additional loss of 20-40 dB) when diffraction loss around or over the building is large. Similarly to reflection attenuation coefficients these losses will be related to building materials, and radio frequency as well as the buildings' internal structure (internal walls). The loss could either be modelled as a series of wall losses (where sufficient data is available), or as loss per metre through the building. Where more than one building blocks the direct path it may be best to ignore this mechanism since then combinations of diffracted, reflected and through building paths should also be considered.

2.1.4 Statistical model

For a given transmitter (Tx) and receiver (Rx) position, the probability that a LoS ray exists between them is given by combining the probabilities that each building lying in the propagation path is below the height of the ray joining the transmitter and receiver at the point where the ray crosses the building. Figure 1 shows the geometry of the situation and defines the terms used in equation (15). This model assumes that the terrain is flat or of constant slope over the area of interest.

The height of the ray at the obstruction point, h_{LoS}, is given by:

$$h_{LoS} = h_{tx} - \frac{r_{LoS}(h_{tx} - h_{rx})}{r_{rx}}$$

(15)

where:

h_{tx} : height above ground of the transmitter

h_{rx} : height of the receiver at the distance r_{rx}

r_{LoS} : distance from the transmitter to the obstacle.

If it is assumed that, on average, buildings are evenly spaced, the number of buildings lying between two points can be estimated. The probability that a LoS ray exists is:

$$P(LoS) = \prod_{b=1}^{b_r} P(\text{building\_height} < h_{LoS})$$

(16)

where b_r is the number of buildings crossed.

For this simple model, three parameters are required:

– α: the ratio of land area covered by buildings to total land area (dimensionless);

– β: the mean number of buildings per unit area (buildings/km^2);

– γ: a variable determining the building height distribution.

For the proposed Rayleigh distribution, the variable γ equates to the most probable (mode) building height. The reason for the distinction between α and β is illustrated in Fig. 4. Both Figs 4a) and 4b) have the same ground area covered and hence the same value of α, but more ray interactions are expected in Fig. 4a) than in Fig. 4b). α alone does not distinguish between the two patterns shown in Fig. 4. If the buildings are of a similar height in both Figs 4a) and 4b), the probability of clearing many small buildings will be significantly less than that of clearing one large building.

FIGURE 4

Two scenarios with the same area covered but different number of ray interactions
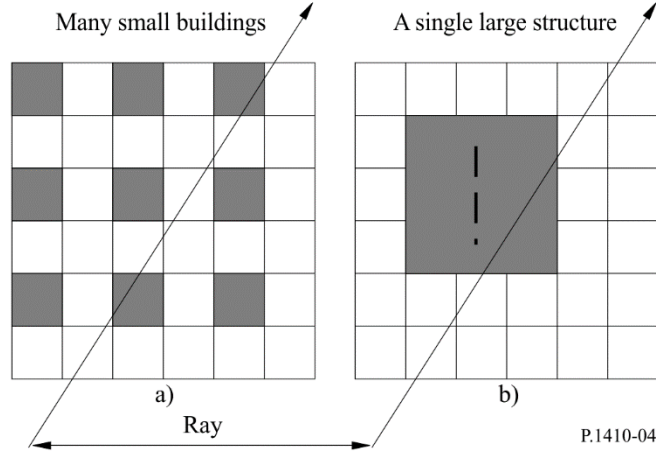
For suburban to high-rise locations α will range from 0.1 to 0.8 and β from 750 to 100 respectively.

The Rayleigh probability distribution $P(h)$ of the height h defines the parameter γ:

$$P(h) = \frac{e^{-\frac{h^2}{2\gamma^2}}\, h}{\gamma^2} \tag{17}$$

2.1.5 Algorithm and computation

Given α, β and γ the LoS coverage is computed as follows:

A ray of length 1 km would pass over $\sqrt{\beta}$ buildings if they were arranged on a regular grid. As only a fraction α of land is covered, the expected number of buildings passed per km is given by:

$$b_1 = \sqrt{\alpha\,\beta} \tag{18}$$

and so for a path of length r_{rx} (km), the number of buildings is:

$$b_r = \text{floor}\,(r_{rx}\,b_1) \tag{19}$$

where the floor function is introduced to ensure that an integer number of terms are included in equation (16).

*To calculate the probability of there being a LoS ray at each range r_{rx}:*

Step 1: Calculate the number of buildings b_r between Tx and Rx points using equation (19).

Step 2: Buildings are assumed to be evenly spaced between the Tx and Rx points, the building distances being given as:

$$d_i = \left(i + 1/2\right)\delta_r \qquad i \in \left\{0,1,....,\left(b_r - 1\right)\right\} \tag{20}$$

where $\delta_r = r_{rx}/b_r$ is the building separation.

FIGURE 5

Location of buildings with respect to Rx in distance r_{rx} from Tx
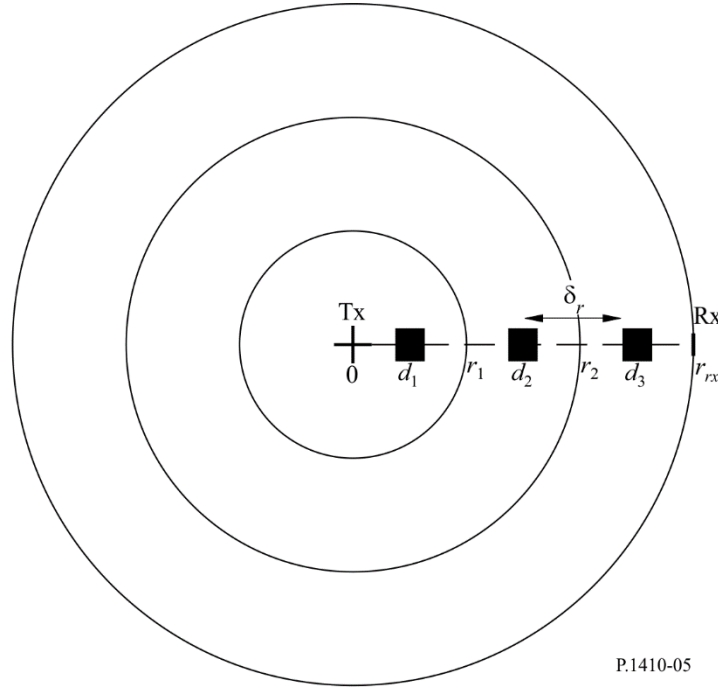
P.1410-05

Step 3: At each d_i the height h_i of a building that would obstruct the LoS ray is given by substituting d_i into equation (15).

$$h_i = h_{tx} - \frac{d_i(h_{tx} - h_{rx})}{r_{rx}} \tag{21}$$

Step 4: The probability P_i that a building is smaller than height h_i is given by:

$$P_i = \int_0^{h_i} P(h)\,\mathrm{d}h \tag{22}$$
$$= 1 - e^{-h_i^2/2\gamma^2}$$

Step 5: The probability $P_{LoS,i}$ that there is a LoS ray at position d_i is given by:

$$P_{LoS,i} = \prod_{j=0}^{i} P_j \qquad j \in \{0,....,i\} \tag{23}$$

Step 6: The cumulative coverage is obtained weighting each $P_{LoS,i}$ with weights W_i dependent on the distance from the transmitter. It accounts for the number of buildings in an annulus being greater at larger distance.

$$W_i = 2i + 1 \tag{24}$$

Step 7: Summing the building weighted probabilities and normalizing by the cumulative annulus area multiplied by building density gives the required coverage for a cell with radius r_{rx}:

$$CP_{r_{rx}} = \frac{\sum_{i=0}^{b_r-1} P_{LoS,i}\, W_i}{b_r^2}$$

(25)

Some limitations are recognized in the current modelling and there are a number of ways in which the model may be extended:

– No terrain variation has been taken into consideration in the model. Clearly variations of even a few metres may have significant effects. Combining the statistical properties of the model with a coarse terrain database, by adding a mean offset to the blockage height for each point tested in the model, would extend the prediction capabilities of the model.

– The density and heights of buildings vary greatly from one region to another and so predictions in one direction should be different from those in another. It is clear from measured building height distributions that the buildings do not fit the simple statistical pattern perfectly. Subdividing the database into smaller regions and assigning each region a set of parameters of its own would go a long way towards addressing this problem.

– In reality, receivers are placed on the rooftops of buildings, so that the distribution of receiver heights follows the same distribution as the building height points. In the model, the receivers were assumed to be at a constant height relative to the ground. An alternative would be to generate receiver heights from the building distribution; this will again be regionally dependent.

– The method derived with the algorithm given gives good coverage estimates when compared with ray-tracing results from ray-tracing on actual databases, see § 2.1.6. The Rayleigh building height distribution has been found accurate for some samples of data where a limited area was considered, e.g. a small town. Furthermore, to get the coverage results as reported in § 2.1.6 it has to be deployed with the building location and path clearance model as given by the step-by-step procedure.

2.1.6 Examples of coverage predictions

The Rayleigh fit was made to the cumulative distribution of rooftop heights found in a suburban location in the United Kingdom (Malvern). For this dataset, the model parameters averaged over the main town region were:

$$\alpha = 0.11; \quad \beta = 750; \quad \gamma = 7.63$$

Figures 6 and 7 show results derived from the model. Figure 6 shows coverage as a function of transmitter height, and Fig. 7 as a function of receiver height.

The model produces predictions with the same basic shape and overall coverage level as the results found from detailed ray tracing simulations. The usefulness of the model is that it can generate predictions of coverage based upon just three parameters which may be estimated for any urban location provided that a little knowledge of the area is available. As more 3D data become available it should be possible to generate tables of parameters for different towns/cities which can be used as a reference when estimating coverage in some unknown site. The model can be used not only to estimate coverage in a single cell, but results from many cells can be combined to produce coverage over large networks including the effects of diversity.

FIGURE 6

**Modelled cumulative coverage for receiver at height of 7.5 m
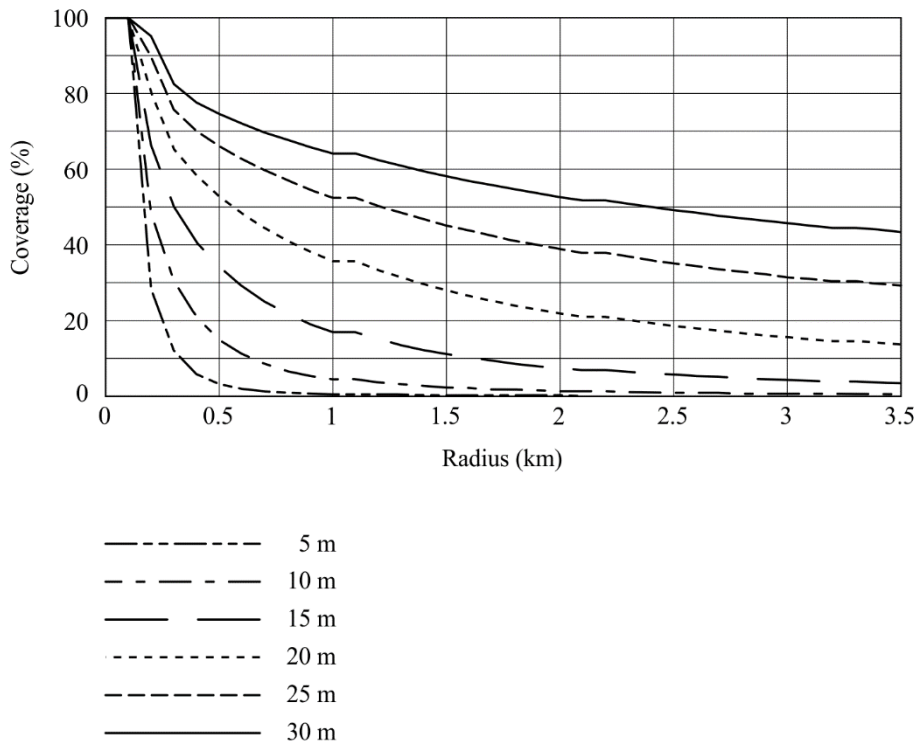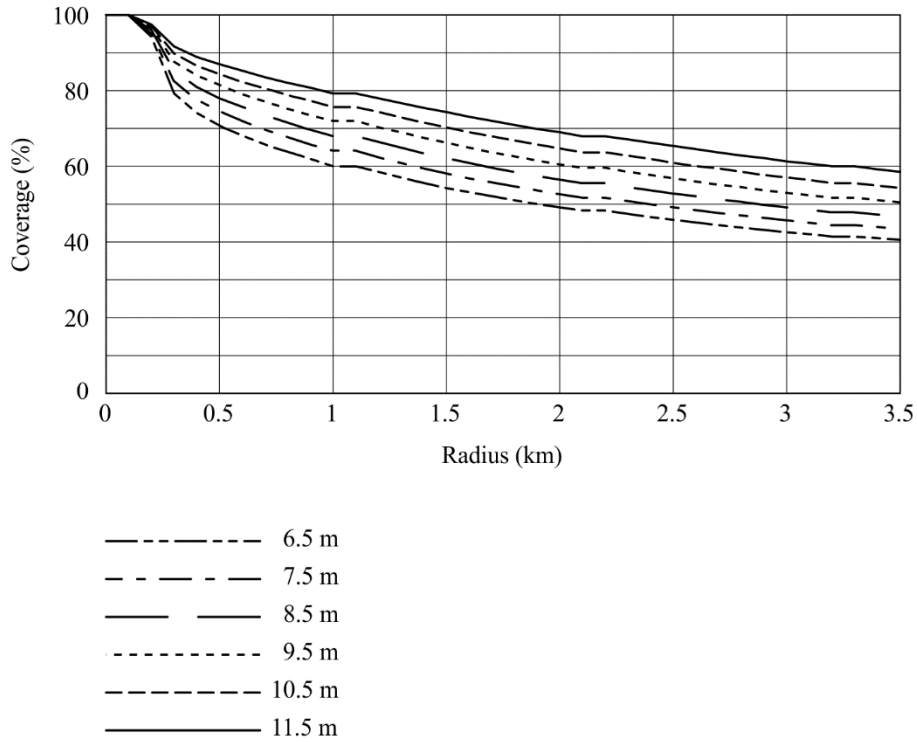and transmitter at heights of 5, 10, 15, 20, 25 and 30 m**

— · — · — · —	5 m
— · — · —	10 m
—— ——	15 m
- - - - - -	20 m
— — — — —	25 m
——————	30 m

P.1410-06

**Modelled cumulative coverage for transmitter at height of 30 m
and receiver at heights of 6.5, 7.5, 8.5, 9.5, 10.5 and 11.5 m**

— · — — · · · ·	6.5 m
— · — · —	7.5 m
——— ———	8.5 m
· · · · · · · · · ·	9.5 m
— — — — — —	10.5 m
———————	11.5 m

P.1410-07

2.1.7 Coverage increase using two or more base stations

A cell architecture that allows receivers to select from more than a single base station provides a significant increase in coverage. For example from ray tracing calculations, for 30 m transmitter antenna heights, the coverage in a 2 km cell increased from 44% for a single base station to 80% for two stations and 90% for four stations, even though the base stations were not specially selected to have good individual visibility.

By assuming that the probabilities of LoS paths to the different base stations of interest are statistically independent, the probability that at least one path exists can be calculated. First each $P_{LoS,i}$ should be calculated from equation (23). Then the probability that at least one path is visible given m possible base stations becomes:

$$P_{LoS,i} = 1 - \prod_{k=1}^{m}\left(1 - P_{LoS,i,k}\right)$$

(26)

By replacing $P_{LoS,i}$ in equation (23) with equation (26) in the procedure in § 2.1.5 the coverage using two or more base stations can be estimated. Note that for each k, Steps 1 to 5 have to be followed where r_{rx} is the distance to each base station.

2.2 Vegetation attenuation

Blockage by trees may severely limit the number of homes to which a service can be provided. It is therefore very important to have a reliable model of the effects and extent of attenuation by vegetation as, for receivers near to the transmitter, the system margin may be such that the signal strength after propagation through a single tree is insufficient for a service.

A ray-trace investigation of six towns in the United Kingdom using databases containing all buildings and trees showed that up to 5% of the buildings within a range of 1 000 m of a central base station were blocked by vegetation. The base station was located on top of the tallest building in the area, typically at 30-40 m above ground and a building was considered unblocked if a line-of-sight path was possible to any test point on that building. The building test points were located on a regular 1 m grid of highest point within the footprint of each building. At range beyond about 1 200 m the vegetation blockage percentage did not change provided the base station height was maintained. At long ranges, owing to Earth curvature other buildings and eventually terrain became the dominant cause of blockage. In a suburban area the vegetation blockage was about 25%.

Measurements were made at 42 GHz to determine the significance of "local tree" attenuation. The mean attenuation was found to be as expected from Recommendation ITU-R P.833 but with significant multipath effects causing deep signal nulls which varied with time as the vegetation moved in the wind. It was found that these multipath nulls could be successfully decorrelated by using two antennas with a separation of ≈60 cm or greater. Closer separations showed greater correlation and larger separations little improvement in decorrelation of attenuation. This suggests that a dual antenna space diversity configuration may allow services to operate in these situations. An experiment at 42 GHz using two antennas separated by 62 cm, demonstrated significant variability of the individual antennas as well as possible diversity improvement. A long-term measurement of propagation through trees in leaf showed that typically 10 dB diversity gain can be obtained.

Tree attenuation is severe at millimetric wavelengths. The attenuation rate depends on tree type, moisture content and path geometry, but a rate of 4-5 dB/m can be used as a guide (although the attenuation does saturate at some value, typically 20-40 dB). It is recommended that the model in Recommendation ITU-R P.833 is used to determine the significance of vegetation attenuation.

2.3 Propagation mechanisms case study

In this section simulation results from a case study using a real urban terrain database. Results showing the dominant propagation mechanisms for coverage and also the statistical distribution of carrier power to interference power ratio (CIR) for an interference scenario are presented.

2.3.1 Description of terrain

The terrain selected is a 2 km by 1 km area of urban Manchester, UK. The area contains three buildings significantly taller than the surrounding buildings. Coverage statistics have been assessed with a transmitter located 15 m above the top of the tallest building. Interference statistics have been assessed with an interfering transmitter on one of the other tall towers. Basic transmission losses have been estimated in a uniform grid at 2 m above the terrain. The points have been subdivided into two sets: rooftop points and street-level points.

2.3.2 Propagation mechanisms modelled

The propagation calculation uses:

–   Recommendation ITU-R P.526 with 1-point diffraction over small scale

–   Diffraction around

–   Building transmission

– Surface permittivity = 5

– Internal building losses = 2.1 dBm

– Reflections and scattering

– Single and double bounce. Non-LOS paths with diffraction/transmission included

– Surface permittivity = 5

– Standard deviation of surface roughness = 0.001 m.

2.3.3 Coverage with varying propagation mechanisms

The extent to which increasing the number of modelled propagation mechanisms changed the coverage predictions at 2.4 GHz is shown in Table 2. Basic transmission loss differences are shown with respect to the 1-point Recommendation ITU-R P.526 predictions.

TABLE 2

Summary of basic transmission losses differences between 1-point Recommendation ITU-R P.452 with various propagation mechanisms

	1-point/Rec. ITU-R P.452			3-point/Rec. ITU-R P.452			Building penetration + horizontal diffraction				
All points	**Clear % LoS**	**% 1st Fresnel**	**% over**	**Clear % LoS**	**% 1st Fresnel**	**% over**	**Clear % LoS**	**% 1st Fresnel**	**% over**	**% through**	**% around**
	45.57	**9.03**	**45.40**	**45.57**	**9.03**	**45.40**	**45.57**	**9.03**	**24.85**	**6.86**	**13.70**
				Mean diff std dev	−3.56 dB 8.42 dB 4 753 points		Mean diff std dev	2.18 dB 5.47 dB 4 753 points			
Only points with difference				Mean diff std dev	−11.62 dB 11.74 dB 1 455 points		Mean diff std dev	10.60 dB 7.51 dB 976 points			

	Specular reflections + scattering + building penetration + horizontal diffraction						
All points	**Clear % LoS**	**% 1st Fresnel**	**% over**	**% through**	**% around**	**% specular reflections**	**% scattering**
	45.57	**8.21**	**17.99**	**3.85**	**8.46**	**15.93**	**0.00**
	Mean diff std dev	5.05 dB 10.45 dB 4 753 points					
Only points with difference	Mean diff std dev	17.93 dB 12.54 dB 1 338 points					

Including the extra propagation mechanisms can have a dramatic effect on the basic transmission loss predictions, averaging almost 18 dB. Whilst this may not be critical for coverage prediction, it would have a significant effect on the performance of an interfered-with system and thus modelling correctly is important.

### 2.3.4   Coverage with varying frequency

Coverage at 2.4 GHz, 5.8 GHz and 28.0 GHz was calculated with all propagation mechanisms modelled. Figure 3 shows the coverage calculated at the three frequencies. The main point of interest is to note that the losses for diffracted paths are far greater at 28 GHz. The 28 GHz however suffers much lower basic transmission losses for many locations. This is due to the scattering mechanism since the surface roughness of buildings introduces far more scattering at higher frequencies.

The percentage breakdown of the dominant propagation mechanisms at each frequency are shown in Fig. 8a). Spectral reflections are especially significant at lower frequencies. Scattering only becomes significant at 28 GHz. Figure 8b) and Fig. 8c) split the results of Fig. 8a) into rooftop and street level locations respectively.

It is useful to further examine the propagation mechanism importance as a function of excess basic transmission loss since, although a particular mechanism may be dominant, for coverage purposes at least, if the excess basic transmission loss is large, it may not be significant. Figure 9 shows the dominant propagation mechanism to each rooftop point at each frequency. This shows the influence of scattering at high frequencies more clearly.

The main points to note from the plots are that spectral reflections and diffraction around can provide significant extra coverage (< 10 dB excess basic transmission loss) at all frequencies. Other mechanisms (building transmission, diffraction over, scattering) are far less significant to the coverage calculation. However, when considering interference even significantly attenuated paths become significant especially when higher order modulation schemes are to be used.
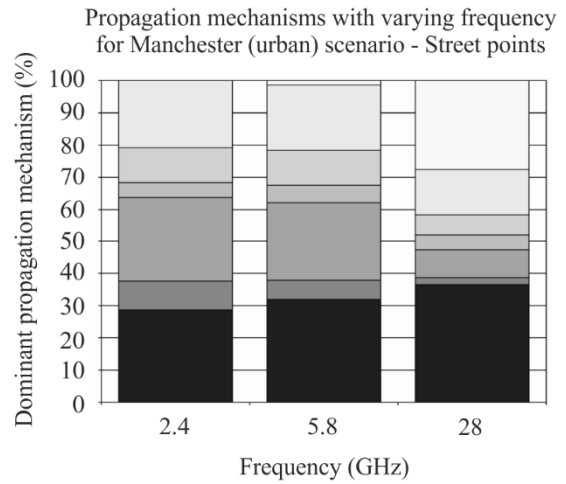
FIGURE 8

Dominant propagation mechanism vs coverage
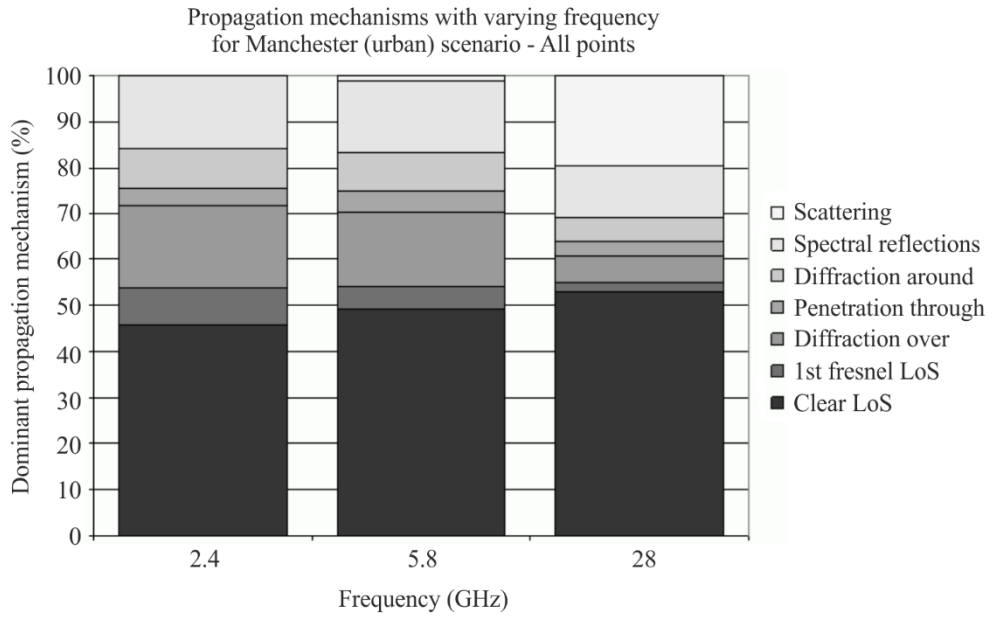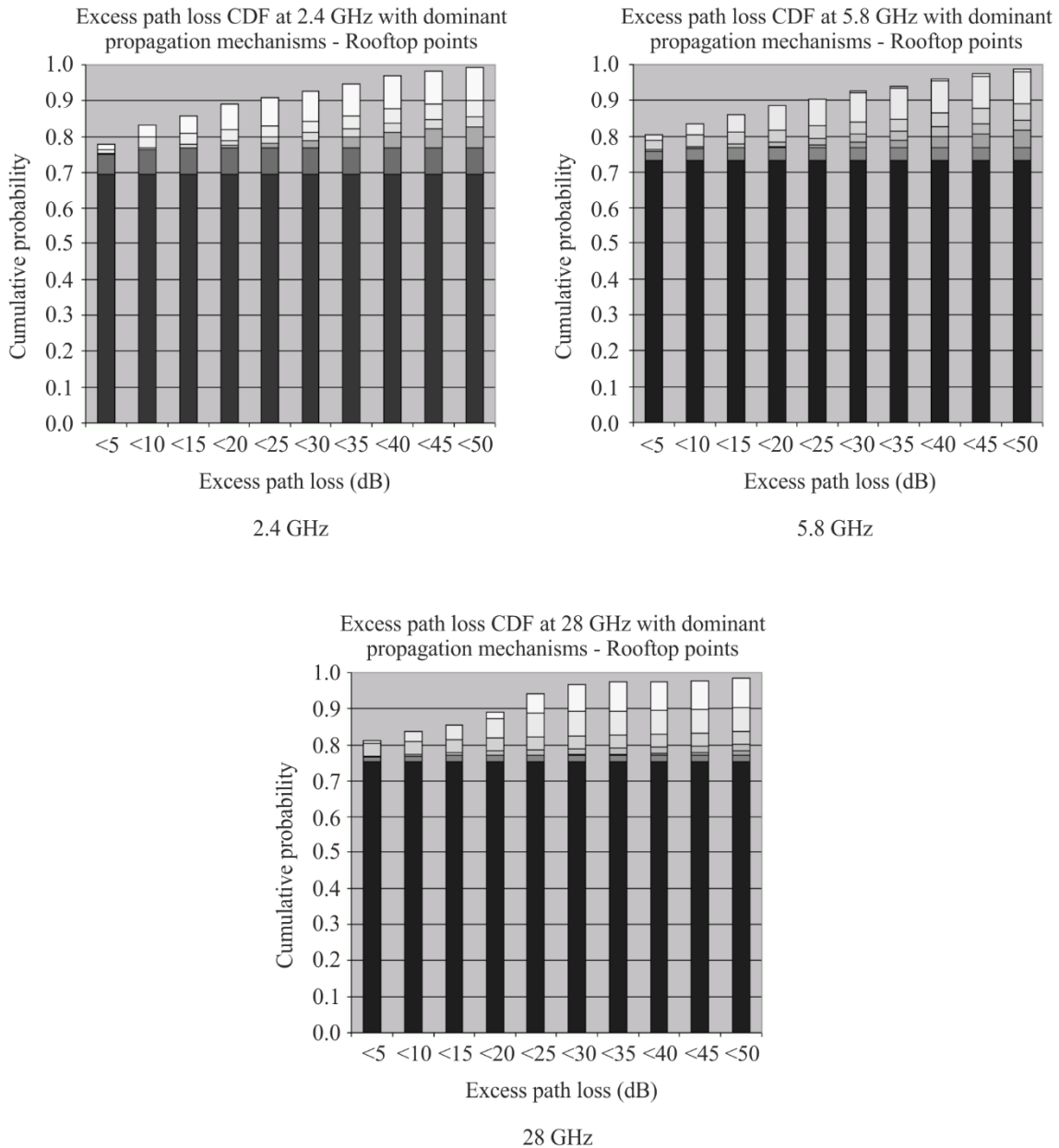

a) All points
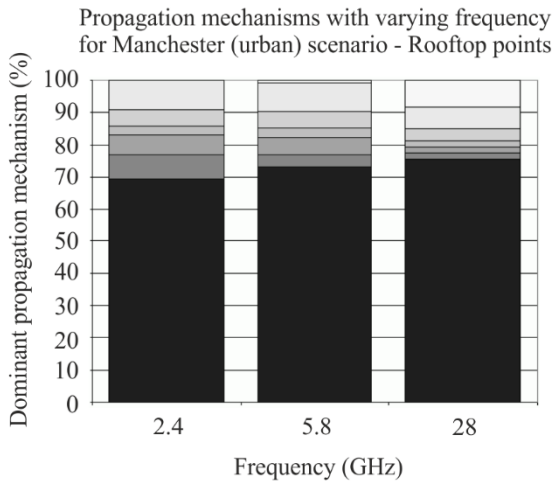
b) Rooftop points only

c) Street level points only

P.1410-08

FIGURE 9

Excess basic transmission loss against dominant propagation mechanisms at rooftop points

2.4 GHz

5.8 GHz

28 GHz

P.1410-09

2.3.5   Summary of case study results

The case study revealed a number of interesting results with regard to the effect of different propagation mechanisms in coverage and interference calculations.

–   At low frequencies specular reflection and diffraction around objects can have a considerable effect on coverage.

–   Scattering was only found significant at 28 GHz. The excess basic transmission losses (generally > 25 dB) attributed to this mechanism make it less significant in providing coverage, though it should be considered in evaluating interference.

–   Inclusion of specular reflections in interference modelling has a significant impact on the interference level predicted, especially when directional antennas are used. For a fixed

network with directional antennas in an urban scenario, reflections should be modelled for accurate interference prediction.

It is important to understand the limitations of the scenario. Firstly the results are applicable to an urban area with high transmitter locations with large elevation angles over the short ranges that were examined. Lower transmitter locations might change the conclusions drawn. It is expected that rural and suburban scenarios would give significantly different results with regard to the breakdown of dominant propagation mechanisms. The absence of large reflective objects would reduce the influence of specular reflection though scattering may still be important. For suburban and rural scenarios inclusion and correct modelling of vegetation data is also very important.

2.4 Basic transmission loss dependence on subscriber station (SS) antenna height

Figure 10 shows the mechanism of the propagation over the rooftops based on a geometrical propagation model. We can divide the height variation of the basic transmission loss due to the base station (BS) – subscriber station (SS) horizontal distance into three regions depending on the arriving wave that is dominant over the entire level. Figure 11 shows the geometry for the calculation of the height variation of the basic transmission loss in the following three regions.

a)   The direct wave dominant region where the BS-SS horizontal distance is very short (Fig. 11(a))

In this region, the direct wave can arrive at any height of the SS antenna. The basic transmission loss and the height variation of the basic transmission loss at the SS are dominated by the propagation loss of the direct wave (LoS region at any height of the SS antenna).

b)   The reflected wave dominant region where the BS-SS distance is relatively short (Fig. 11(b))

In this region, a strong reflected wave as a one- or two-time reflected wave and diffracted wave can arrive at any height of the SS antenna in the non-line-of-sight (NLoS) region. The propagation loss of the minimum-time reflected wave arriving at any height of the SS antenna is lower than that of the diffracted waves in the NLoS region. The basic transmission loss and height variation of the basic transmission loss at the SS in this region are dominated by the reflected waves. The basic transmission loss in the relatively near region corresponds to the direct, one-, and two-time reflected wave components at the minimum height where the direct, one-, and two-time reflected waves arrive at the SS.

c)   The diffracted wave dominant region where the BS-SS distance is relatively long (Fig. 11(c))

In this region, a strong reflected wave as a one- or two-time reflected wave can only just barely arrive at the SS antenna in the NLoS region where the SS antenna height is lower than that of the surrounding buildings, and only weak many-time reflected waves and diffracted waves can arrive at the SS antenna. The propagation loss of the minimum-time reflected wave arriving at the SS becomes higher than that for the diffracted wave. The basic transmission loss and height variation of the basic transmission loss at the SS in the far region are dominated by the diffracted waves from the edge of the building roof. The basic transmission loss and height variation of the basic transmission loss at the SS nearly correspond to those for the diffracted wave.

FIGURE 10

Mechanism of propagation over rooftops based on geometrical propagation model
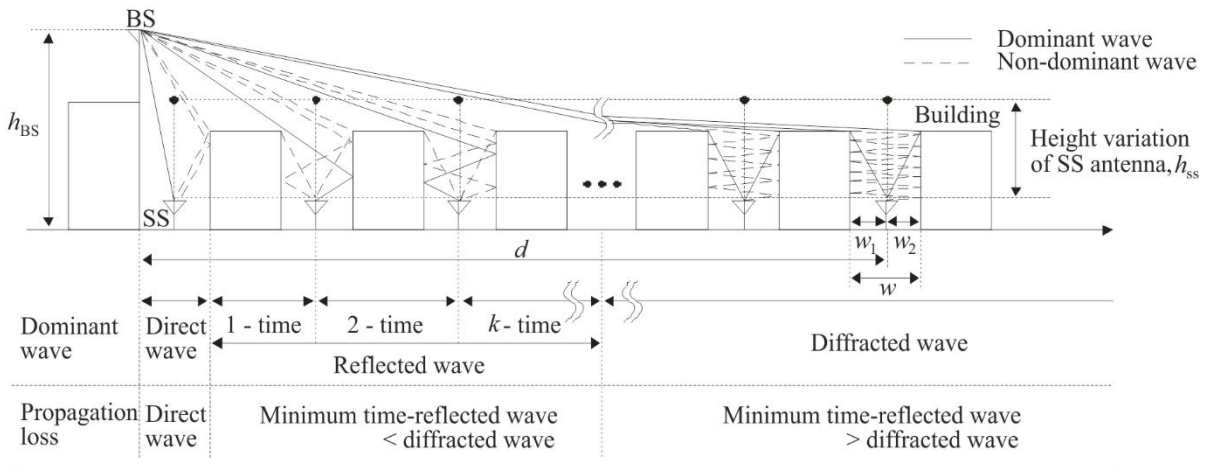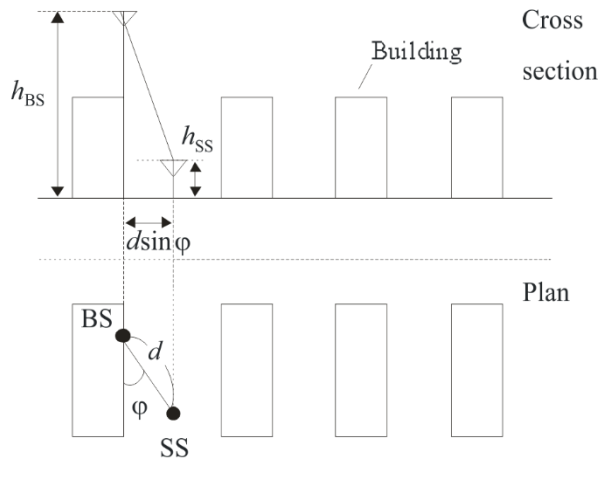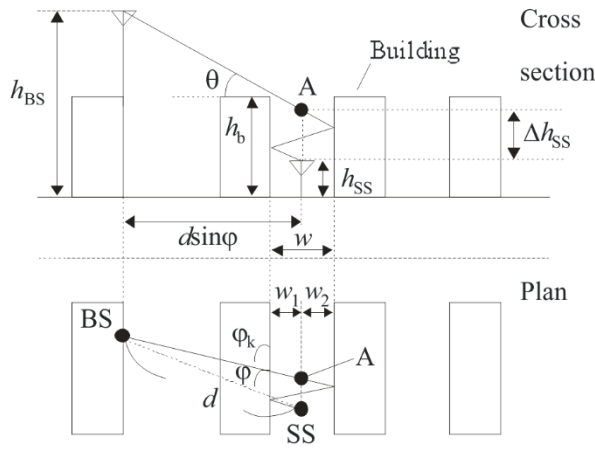

P.1410-10

FIGURE 11
Propagation model based on dominant waves that influence height variation of basic transmission loss
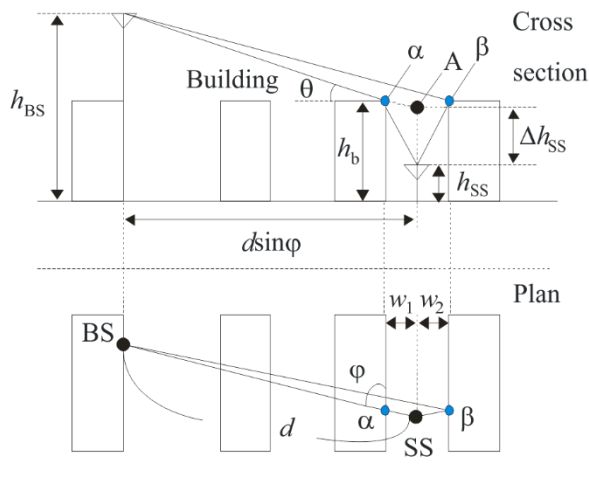
(a) Direct wave dominant region where BS-SS horizontal distance is very short (LoS)

(b) Reflected wave dominant region where BS-SS distance is relatively short

(c) Diffracted wave dominant region where BS-SS distance is relatively long

P.1410-11

The relevant parameters for each situation are given hereafter:

f: frequency (GHz)

φ : angle between building row and line of visibility/LoS (degrees)

h_{BS}: base station antenna height (m)

h_{SS}: subscriber station antenna height (m)

Δh_{SS}: depth to the shadow region (m)

h_b: average building height (m)

w: distance between buildings (m)

d: horizontal distance between antennas (m).

Here, this model is valid for the following:

f: 2 to 30 GHz

φ: 10 to 90 degrees

h_{BS}: up to 70 m (higher than h_b)

h_{SS}: 2 to (h_b+3) m

w: 10 to 25 m

d: 10 to 5 000 m.

NOTE – The range of the antenna height of the SS covers continuously from LoS to NLoS regions.

Based on these propagation mechanisms, the loss due to the SS antenna height between isotropic antennas can be divided into three regions in terms of the dominant arriving waves at the SS. These are the direct wave dominant region (LoS region), reflected wave dominant region (NLoS region), and diffracted wave dominant region (NLoS region). The height variation is nearly equal to zero in the LoS region. On the other hand, in the NLoS region the height variation in the basic transmission loss depends on the dominant arriving wave. Therefore, the excess loss of the NLoS region from that for the LoS region, $L(\Delta h_{SS})$ can be defined by:

$$L(\Delta h_{SS}) \cong \min\{L_R(\Delta h_{SS}), L_D(\Delta h_{SS})\} \quad \text{(dB)} \tag{27}$$

Here, $L_R(\Delta h_{SS})$ and $L_D(\Delta h_{SS})$ are the excess loss due to the arriving reflected waves and the arriving diffracted waves in the NLoS region, respectively. The $L_R(\Delta h_{SS})$ and $L_D(\Delta h_{SS})$ are expressed as follows.

When:

$$\Delta h_{SS,k} \le \Delta h_{SS} < \Delta h_{SS,k+1}$$

$$L_R(\Delta h_{SS}) = L_R(\Delta h_{SS,k}) + \frac{L_R(\Delta h_{SS,k+1}) - L_R(\Delta h_{SS,k})}{\Delta h_{SS,k+1} - \Delta h_{SS,k}} \cdot (\Delta h_{SS} - \Delta h_{SS,k}) \quad (k = 0,1,2,3,\cdots)\text{(dB)} \tag{28}$$

$$\Delta h_{SS,k} = \frac{2kw \cdot (h_{BS} - h_b)}{2d \cdot \sin\varphi - w} \quad \text{(m)} \tag{29}$$

$$L_R(\Delta h_{SS,k}) \approx 20\log\left(\frac{d_{kp}}{d_{0p} \cdot R^k}\right) \quad \text{(dB)} \tag{30}$$

$$R \approx 0.4 \, (\text{if the model applies to } h_{bs} > 70 \text{ m, } d > 5\,000 \text{ m, } R = 0.33)$$

$$d_{kp} = \frac{1}{\sin \varphi_k} \cdot \sqrt{(d \cdot \sin \varphi + kw)^2 + \left\{ h_{BS} + \Delta h_{SS,k} - h_b + \frac{w \cdot (h_{BS} - h_b)}{2d \cdot \sin \varphi - w} \right\}^2} \quad (\text{m}) \tag{31}$$

$$\varphi_k = \tan^{-1}\left(\frac{d \sin \varphi}{d \sin \varphi + kw} \cdot \tan \varphi \right) \quad (\text{degrees}) \tag{32}$$

$$L_D(\Delta h_{SS}) \approx \begin{cases} \{5.8947 \cdot \log(f) + 0.31519\} \times \Delta h_{SS}^{(-0.003559 \cdot f + 0.65122)} & (0 \text{ m} \leq \Delta h_{SS} < 1 \text{ m}) \\ \{3.7432 \cdot \log(f) + 19.245\} \cdot \log(\Delta h_{SS}) + 5.8947 \cdot \log(f) + 0.31519 & (1 \text{ m} \leq \Delta h_{SS} < 10 \text{ m}) \\ 24.5 \cdot \log(\Delta h_{SS}) + 9.6379 \cdot \log(f) - 4.93981 & (10 \text{ m} \leq \Delta h_{SS}) \end{cases} \quad (\text{dB}) \tag{33}$$

$$\Delta h_{SS} = h_b - h_{SS} - \frac{w(h_{BS} - h_b)}{2d - w} \quad (\text{m}) \tag{34}$$

* If Δh_{SS} becomes negative, that is, a LoS condition arises between the BS and SS antennas, -6 dB is given as the $L(\Delta h_{SS})$ regardless of the SS antenna height because $L(\Delta h_{SS})$ is normalized by the basic transmission loss at the boundary between the LoS and NLoS regions. R is the reflection coefficient for a wall surface of a building in the microwave band and is specified as -8 dB regardless of the incident angle, which indicates the mean value obtained from the measured results.

2.5 Basic transmission loss prediction method considering height gain at SS

The method described in § 2.4 predicts the relative height variation in the basic transmission loss with respect to the SS antenna height. We can also predict the basic transmission loss itself by considering together the height gain at the SS at an arbitrary SS antenna height using the calculation method described in § 2.4, and the conventional basic transmission loss prediction method for the over-rooftop NLoS environment such as in Recommendation ITU-R P.1411.

The basic transmission loss, $L(h_{ss})$, at the target SS antenna height, h_{ss} (when h_{ss} is beyond the upper range defined in the basic transmission loss prediction method for the over-rooftop NLoS environment such as Recommendation ITU-R P.1411), can be calculated as indicated below:

1) Basic transmission loss calculation at a low SS antenna height, h_0

   The basic transmission loss, $L(h_0, d)$, with a certain SS antenna height, h_0, and the target BS-SS distance, d, is calculated using the conventional basic transmission loss prediction method for an over-rooftop NLoS environment such as Recommendation ITU-R P.1411.

2) Height gain calculation when the SS antenna height is h_{ss} based on h_0.

   Excess loss in the NLoS region compared to the LoS region, when the SS antenna height is h_0 and h_{ss}, can be calculated using the height gain prediction method described in § 2.4 as $L(\Delta h_0, d_h)$ and $L(\Delta h_{SS}, d_h)$, respectively,

   where d_h is the horizontal distance between the BS and SS, and Δh_0 and Δh_{SS} are the depths to the shadow region from the LoS region when the SS antenna height is h_0 and h_{ss}, these are derived as follows:
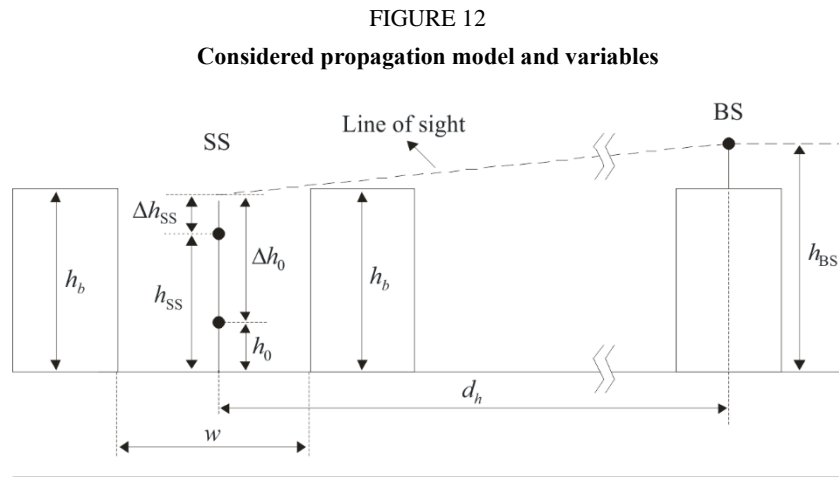
$$d_h = \sqrt{d^2 - \left(h_{BS} - h_0\right)^2} \tag{35}$$

$$\Delta h_0 = h_b - h_0 - \frac{w\left(h_{BS} - h_b\right)}{2d - w} \tag{36}$$

$$\Delta h_{SS} = h_b - h_{SS} - \frac{w\left(h_{BS} - h_b\right)}{2d - w} \tag{37}$$

h_{BS}, h_b, and w are defined in § 2.4, and are shown in Fig. 12.

3)   Basic transmission loss calculation when SS antenna height is h_{ss}, $L(h_{ss})$,

$$L\left(h_{SS}\right) = L\left(h_0, d\right) - L\left(\Delta h_0, d_h\right) + L\left(\Delta h_{SS}, d_h\right) \tag{38}$$

FIGURE 12

Considered propagation model and variables

P.1410-12

2.6   General advice

Some general trends have been noted based on several databases from Northern Europe. Ray tracing has been used to calculate coverage (based on the level of building and vegetation blockage between the base station and the user premises) as a function of transmitter and receiver antenna heights, the advantage of multiple server diversity, and the significance of vegetation blockage. General points are:

–   Coverage can be very site-specific, especially if topographic features or exceptional building blockage near the transmitter occur. However, investigations at several different urban/suburban sites gave coverage figures of 40-60% for a 2 km cell from a 30 m transmitter mast.

–   Coverage increases by 1-2% for each metre of base station mast height increase.

–   Coverage increases by 3-4% for each metre of user premises mast height increase.

–   A cell architecture that allows receivers to select from more than a single base station provides a significant increase in coverage. For example, for 30 m transmitter antenna heights, the coverage in a 2 km cell increased from 44% for a single base station to 80% for two stations and 90% for four stations, even though the base stations were not specially selected to have good individual visibility.

# 3 Effects of precipitation on availability

Once it has been established that a user has an unobstructed LoS to the base station with an adequate free-space system margin, it is then necessary to calculate the percentage of the time that the service will be available when precipitation effects are taken into account.

For any link in the service area of the base stations the availability under precipitation conditions can be estimated using the methods in Recommendation ITU-R P.530.

3.1 Simultaneous area coverage

Since rain is non-uniform in two dimensions horizontally, the one-dimensional model of Recommendation ITU-R P.530 for non-uniform rain on point-to-point links cannot be applied to point-to-area situations. This two-dimensional non-uniformity can be taken into account by applying an average rainfall rate distribution for the rain cell under investigation. With a centrally-fed cell size of radius L, the illustration in Fig. 13 indicates the equivalent area determined by the radius d_0 covered at the chosen percentage of time.

FIGURE 13

Diagram of the centrally-fed cell showing the radius of the equivalent coverage area under rain conditions
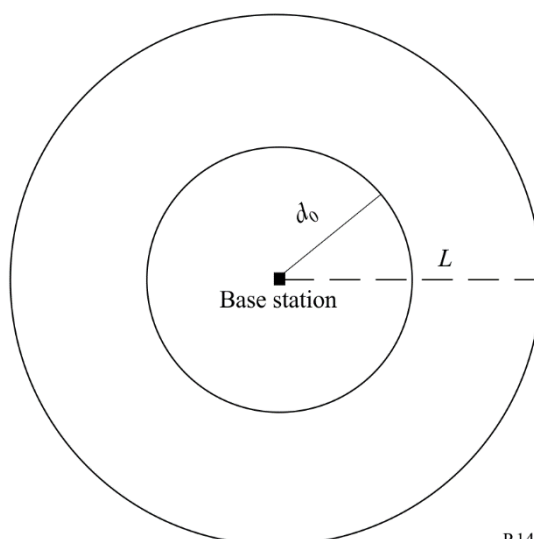
A procedure to predict area coverage has been developed, based on radar measurements from the United Kingdom of rainfall over a two-year period.

For a centrally-fed cell with radius L (km) and system fade margin F (dB) at the edge:

Step 1: Obtain the area-averaged rainfall rate $R_a(p)$ exceeded for $p\%$ of the time from where R is the point rainfall rate for the area.

$$R_a = \left(0.317L^{0.06} + 1\right)R^{1-0.15L^{0.2}} \tag{39}$$

An example of this parameter is given in Table 3 for radar-based data obtained in the United Kingdom. With respect to the point rainfall rate it can be noted that the area-averaged rainfall rate is reduced very little at the 0.1% exceedance level, by about one third at the 0.01% level and by about one half at the 0.001% level for a circular area within 2.5 km radius.

Step 2: Find the cut-off distance d_0 for $p\%$ of an average year by solving equation (39) for d numerically.

$$k\, R_a^\alpha(p)\, d\left(1.5 + \left(1.1\,(2d^{-0.04} - 2.25)\right)\,\log(R_a(p))\right) + 20\log(d/L) = F \qquad (40)$$

where k and α are parameters determining the specific rain attenuation found in Recommendation ITU-R P.838. The term $(1.5 + (1.1\,(2d^{-0.04} - 2.25))\,\log(R_a(p)))$ represents the path reduction factor applicable for the area calculations.

Step 3: For the cut off distance $d_0 \propto (L, p, F)$, the area coverage for this cell is:

$$C(L, p, F) = 100\left(\frac{d_0}{L}\right)^2 \qquad \% \qquad (41)$$

In Fig. 14 the results of the procedure given by equations (39), (40) and (41) are shown for two centrally fed cells of 2.5 km and 5 km radius and for two systems, using vertical polarization at 42 GHz, with 10 dB and 15 dB rain attenuation margin at the edge of the cell. Here it is also assumed that the transmitter antenna gain is equal for all users. Free-space loss is taken into account in the calculations (equation (40)).

TABLE 3

**Point and area average rainfall rate obtained from a
two-year radar data set in the United Kingdom**

Percentage of time	Point rainfall rate, R (mm/h)	Area-averaged R (mm/h)	
		Radius = 2.5 km	**Radius = 5 km**
0.001	65.6	36.0	33.0
0.003	46.2	29.0	23.4
0.01	29.9	19.4	17.1
0.03	18.1	16.3	12.6
0.1	9.8	9.5	8.5
0.3	5.0	4.9	4.8
1	2.0	2.1	2.1

FIGURE 14

Application of the procedure at the location, 1.5° West, 51° North

P.1410-14
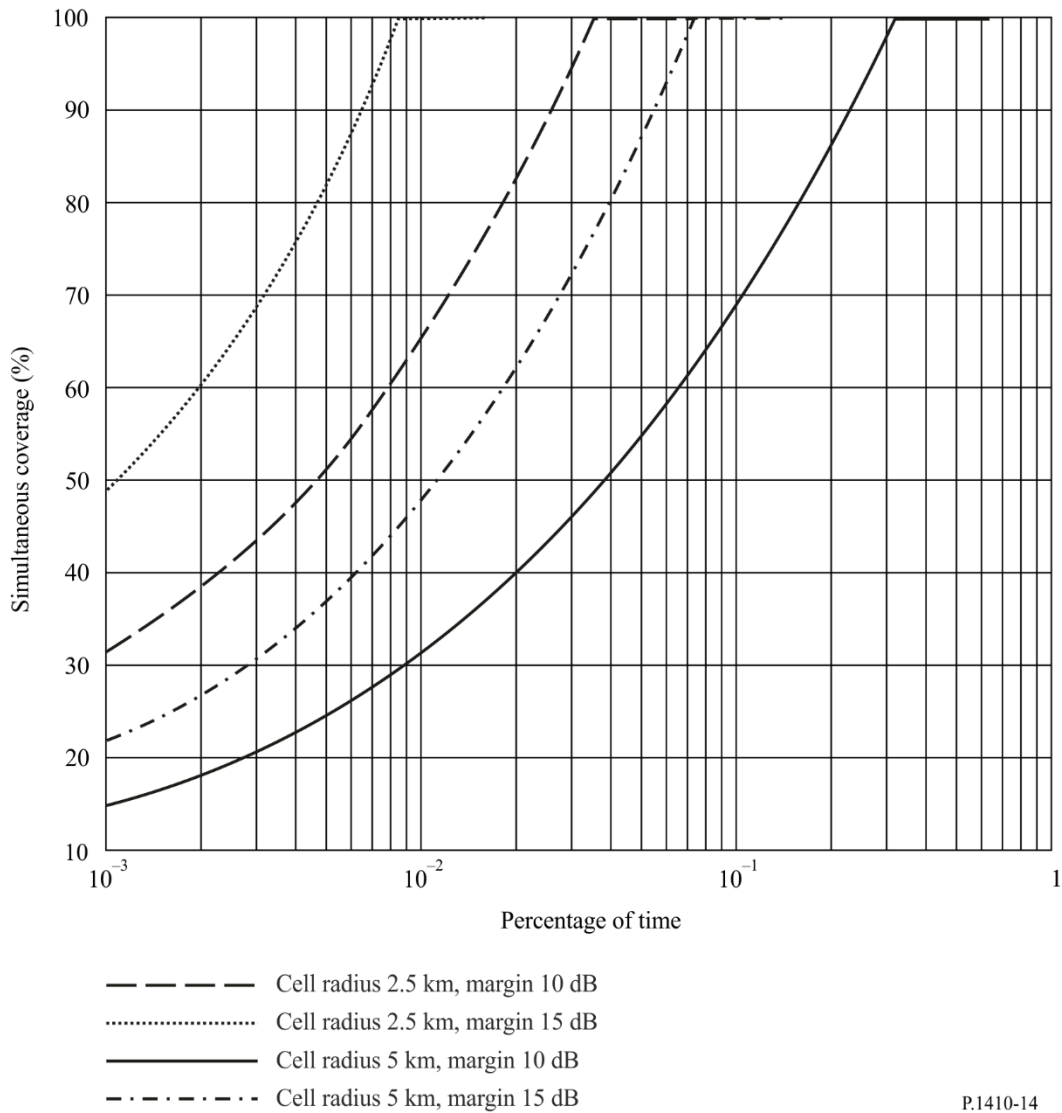
3.2 Route diversity improvement

Precipitation varies considerably in time and in space both vertically and horizontally. For a single link between two terminals, this variability is reflected in the current modelling e.g. by using an effective path length. Assume that a user can connect to two or more base stations at any instant of the time. This section describes how much the availability will be improved if such a system is installed.

A common node star-like network consisting of two transmitters and one receiver taking the two path lengths to be the same is assumed, where angle separation φ ranges from 0° to 360°.

Because rain is horizontally non-uniform, the attenuation statistics for the single path and the two diversity paths are different. Figure 15 shows typical path attenuation statistics for an unprotected path and the combined diversity paths. The improvement due to the angle separation, which can be expressed as the diversity improvement $I(A_i)$ or the diversity gain $G(A_i)$, with reference to one of the two alternative paths $i=1,2$ (unbalanced diversity configuration), is defined as:

$$I(A_i) = \frac{P(A_i)}{P_d(A_i)}, \qquad i = 1,2 \qquad (42)$$

$$G(A_i) = A(t) - A_d(t), \qquad i \ 1,2 \qquad (43)$$

where $P_d(A_i)$ is the percentage of time in the combined diversity path with a fade depth larger than A_i and $P(A_i)$ is the time percentage for the unprotected path. Similarly, $A_d(t)$ is the fade depth in the combined diversity path occurring in time percentage t and $A(t)$ is for the unprotected path.

FIGURE 15

Example of attenuation statistics of path-angle diversity

P.1410-15
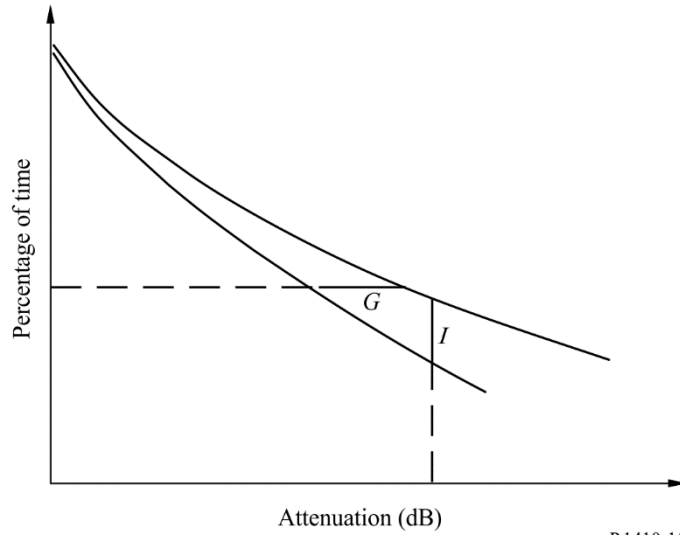
The necessary steps for deriving the diversity improvement I and the diversity gain G are the following:

Step 1: Approximate the annual distribution of rain attenuation A_i (dB) over each path $i = 1,2$ by employing the lognormal distribution:

$$P(A_i) = \frac{1}{2}\operatorname{erfc}\left(\frac{\ln A_i - \ln A_{mi}}{\sqrt{2}S_{ai}}\right) \qquad (44)$$

where $\operatorname{erfc}(x) = 2/\sqrt{\pi} \int_x^\infty e^{-z^2}\, dz$ is the complementary error function. To calculate A_{mi} and S_{ai}, a fitting procedure over either available local measurements or the rain attenuation distribution in § 2.4.1 of Recommendation ITU-R P.530 is recommended. This procedure is detailed in Annex 2 of Recommendation ITU-R P.1057.

Step 2: Determine the rain inhomogeneity constant D_r, that is the distance in km the correlation coefficient becomes equal to $\sqrt{2}/2$. A simple rule for calculating D_r depends on the absolute latitude |*lat*| of the location:

$$D_r = 0.644\ln\left(|lat|\right) - 1.02, \quad 5° \le |lat| \le 90° \qquad (45)$$

Step 3: Determine the characteristic distance of the rainfall area as $D_c = 20\text{x } D_r$.

Step 4: Evaluate the spatial parameter H_i, $i = 1,2$, over each of the alternative path of length L_i:

$$H_i = 2L_i D_r \sinh^{-1}\left(L_i/D_r\right) + 2D_r^2\left(1 - \sqrt{\left(L_i/D_r\right)^2 + 1}\right), \quad i = 1,2 \tag{46}$$

Step 5: Employ a numerical integration method to evaluate the spatial parameter H_{12} between the two paths:

$$H_{12} = \int_0^{L_1}\int_0^{L_2} \rho_0(d)\, d\ell_1 d\ell_2 \tag{47}$$

where:

$$\rho_0(d) = \begin{cases} \dfrac{D_r}{\sqrt{D_r^2 + d^2}} & d \le D_c \\[3mm] \dfrac{D_c}{\sqrt{D_r^2 + D_c^2}} & d > D_c \end{cases} \tag{48}$$

and the distance of two points of the alternative paths forming an angle φ is given by:

$$d^2 = l_1^2 + l_2^2 - 2l_1 l_2 \cos\varphi, \, 0 < l_1 \le L_1, \, 0 < l_2 \le L_2 \tag{49}$$

Step 6: Calculate the correlation coefficient of rain attenuation:

$$\rho_a = \frac{1}{S_{a1}S_{a2}} \ln\left[\frac{H_{12}}{\sqrt{H_1 H_2}}\left(e^{S_{a1}^2} - 1\right)^{1/2}\left(e^{S_{a2}^2} - 1\right)^{1/2} + 1\right] \tag{50}$$

Step 7: The joint probability of the combined (unbalanced) diversity configuration exceeding a fade depth of A_i is given by:

$$P_d(A_i) = \frac{1}{2}\int_{u_2}^{\infty} \frac{1}{\sqrt{2\pi}} \exp\left(-\frac{u^2}{2}\right)\operatorname{erfc}\left(\frac{u_1 - \rho_a u}{\sqrt{2}\sqrt{1 - \rho_a^2}}\right) du \tag{51}$$

where:

$$u_i = \frac{\ln A_i - \ln A_{mi}}{S_{ai}}, \, i = 1,2 \tag{52}$$

Step 8: The diversity improvement I at the reference attenuation level A_i is obtained based on the definition given in equation (42).

Step 9: The diversity gain G at the reference percentage t is obtained based on the definition given in equation (43), after reversing equations (44) and (51) (see Note 1).

NOTE 1 – For reversing equation (51), numerical analysis must be applied.

4 Propagation channel distortion

In this section, the instantaneous effects of vegetation dynamics and building and terrain multipath on the propagation channel are considered. Because of the sparse data currently available, the results from available measurements are given for guidance. Information on signal variability, the standard deviation, for propagation through moving vegetation can be found in Recommendation ITU-R P.833.

## 4.1 Frequency selective vegetation attenuation

Measurements with a filter bank on a 34 MHz bandwidth transmission have been performed to investigate the possible occurrence of frequency selective fading across the channel. The filter bank consisted of eight channels of 1.6 MHz bandwidth (–3 dB) separated by 3 MHz and placed in the middle of the channel.

The measurement was performed behind a birch tree at a distance of 15 m. The sampling interval was 100 ms. Since there was no wind during the measurement period, windy conditions were simulated using ropes tied to the tree. Figure 16 shows a comparison of the signal level of the channels during very windy conditions. The small level of variation seen across the channel suggests that there is no major frequency selective fading. The time variation of the signal level might therefore be due to variation in obstruction or in the density of branches and leaves in between the receiver and the transmitter, or, due to multipath where the propagation time differences are very small.

To further test the observations an experiment was set up using a maximum power combiner (MPC) and two individual antennas separated by 72 cm. A Moving Pictures Experts Group-2 (MPEG-2) TV test transmission was made at 42 GHz using the satellite digital video broadcasting (DVB-S) format quadrature phase shift keying (QPSK) 1/2 rate forward error correction (FEC). The signals from each antenna as well as the combined signals through the maximum power combiner were fed into three DVB-S set-top boxes and video monitors. The geometry was arranged so that both antennas received signals through moving tree branches. Both single antenna DVB-S systems suffered regular packet loss. The packet loss rate was too severe to be corrected by the decoder causing frequent loss of video. Conversely the maximum power combined signal suffered much lower packet losses and the MPEG-2 decoder was therefore able to compensate and the video remained stable.

FIGURE 16

Comparison of the signal level of the channels during very windy conditions

P.1410-16
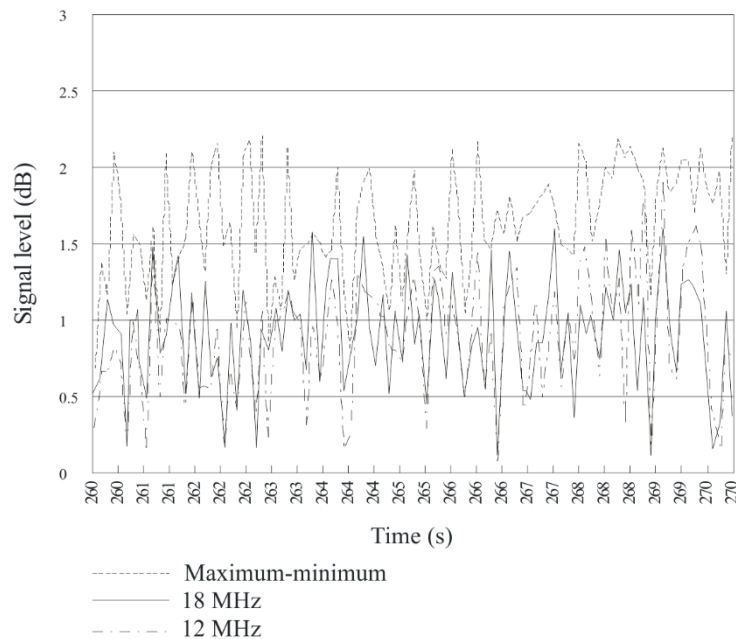
4.2 Multipath from reflections

4.2.1 Results from ray-tracing

Ray-trace simulations have shown that the multipath problem appears to be slight in the conditions under which the system will be operating. The very narrow receiver antenna beamwidth causes the majority of multipath signals to be very heavily attenuated. Only the very shallow grazing rays from nearby rooftops and the ground enter the receiver with an appreciable magnitude. A consequence of this is that the delay-spread values found from simulations are very low.

Diffracted rays have not been considered during ray-trace simulations, but earlier work found that there were very few positions which were able to make use of diffracted rays and consequently, there are likely to be few locations where the diffracted rays are a major source of interference.

Example ray-trace calculations of the delay spread for the receiver locations using a large database (from Oxford in the United Kingdom) show extremely small values, owing to the very low levels of multipath. The average r.m.s. delay spread was found to be around 0.01 ns which corresponds roughly to a coherence bandwidth of 15 GHz. This should not cause any problems to a broadband radio access system. It is unlikely that the true r.m.s. delay spread is as low as this in reality due to the diffracted rays mentioned above, but a coherence bandwidth of up to 5 GHz may still be realistic. The standard deviation of r.m.s. delay-spread is around 0.01 ns.

4.2.2 Results from measurements

Building reflections may be regarded both as a possibility of shadow area fill-in and as harmful multipath. Some observations using an 80 MHz frequency sweep showed that a 9% increase in the number of locations receiving an adequate signal for coverage could be obtained by the inclusion of reflected signals. However, one should note that there are several problems in using reflected signals to provide a service. Firstly, the signal must be stable, which means that the signal incident upon the reflecting object must be a LoS path. If any part of the path is through vegetation or across a path likely to be blocked by moving traffic, the resulting signal will exhibit time variability. Secondly, the reflecting object itself must be permanent and stable.

The extent and roughness of the reflecting building surface has a dramatic effect on the frequency response of the channel. Figure 17 shows the measured channel response of three different reflected signals: one from a factory window, one from the chimney of a terraced house (including a mounted Yagi TV aerial) and one reflected by the corrugated metal wall of a large retail building. It should be noted for the latter building that the corrugated wall gave an extended reflection in angle rather than a single specular reflection. The distance of the sites from the transmitter were 1.34 km, 1.57 km and 616 m respectively.

FIGURE 17

Frequency response for measured reflections at three different locations
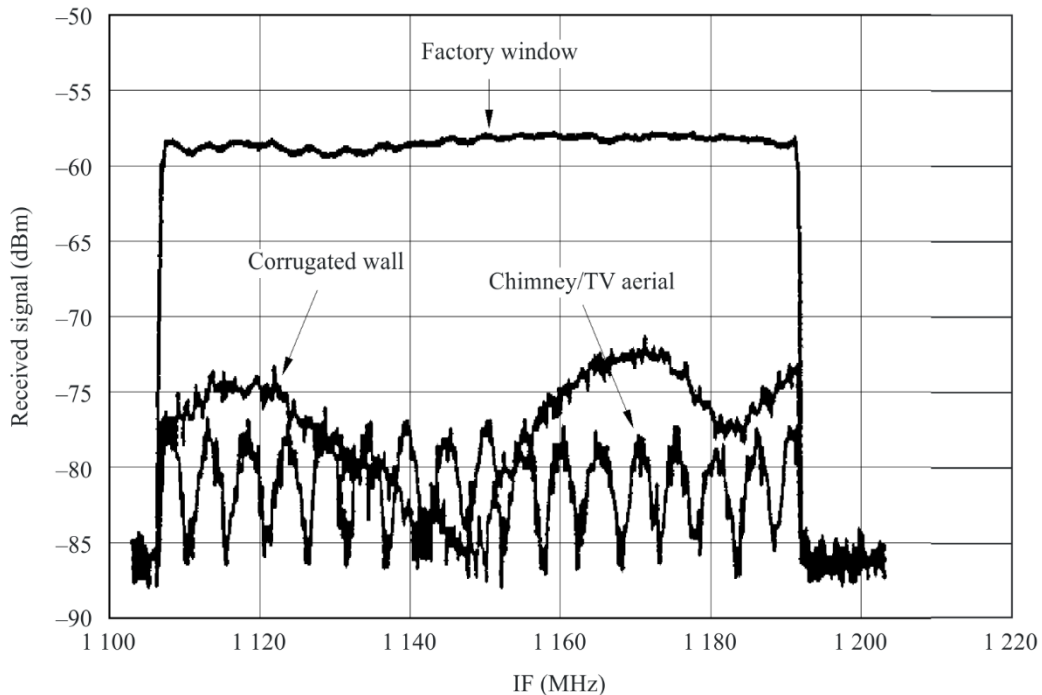

P.1410-17

One can see that the factory window gives a reasonably flat frequency response, since it behaves as a flat mirror and consists of only a single specular component. However, the corrugated wall and chimney show a distinct ripple, corresponding to path length differences (assuming a two-ray model) of 6 m and 60 m, respectively. For the chimney reflection, this large path length may be due to the combination of the reflection from another object some 30 m or so behind the chimney. For the case of the corrugated wall, the 6-mentre path length difference is achievable from different parts of the wall itself, since the whole building could contribute reflected signals, not just the small specular region.

Wideband spectrum measurements were carried out in a suburban area in both the 5 GHz and 25 GHz bands. The occupied frequency band of the transmission spectrum is 26 MHz and the 10 MHz range of the center part of the spectrum is almost flat. In each spectrum, the maximum in-band amplitude dispersion can be calculated from the maximum level and the minimum level in the 10 MHz range of the center part of the spectrum. Assuming a two-wave interference model, the ratio (D/U) of the D-wave such as a direct wave and the U-wave such as reflected wave is an important factor in evaluating the in-band amplitude dispersion. The in-band amplitude dispersion at a terminal is affected by the shadowing caused by obstacles such as the surrounding houses and trees. Assuming that the level of the U-wave is constant, it can be said that the D/U value of the propagation path is 20-30 dB. This indicates that if we use a terminal antenna with an antenna gain of approximately 15 dBi and obtain a shadowing of greater than 20 dB, the in-band amplitude variation has a harmful dispersion. The gain of the directional antenna affects the level of suppression of the interference waves. The D/U value can be assumed to be 50 dB for an antenna with the gain for 32 dBi and 30 dB for an antenna with the gain for 12 dBi. The difference in the gains of the two antennas corresponds to the difference in the above D/U values.

Frequency sweep measurements using a vertically polarized 26 GHz signal taken with reflection angles in the range of 87.5° to 89 (i.e. nearly normal to the wall surface) showed a median attenuation of 7.5 dB. The transmitter and receiver were co-located. The distances to the walls ranged from 37 m

to 402 m. Four buildings were used where the wall surface consisted of glass, tile, and metal with unevenness ranging from 3 cm to 75 cm. Note that the electric field vector was parallel to the walls. A cumulative distribution of the reflection loss is shown in Fig. 18. The standard deviation of the discrepancy of the measurements relative to the Rayleigh distributions was found to be σ = 0.53 dB.

FIGURE 18

Cumulative distribution of measured building wall reflection loss at 26 GHz

P.1410-18
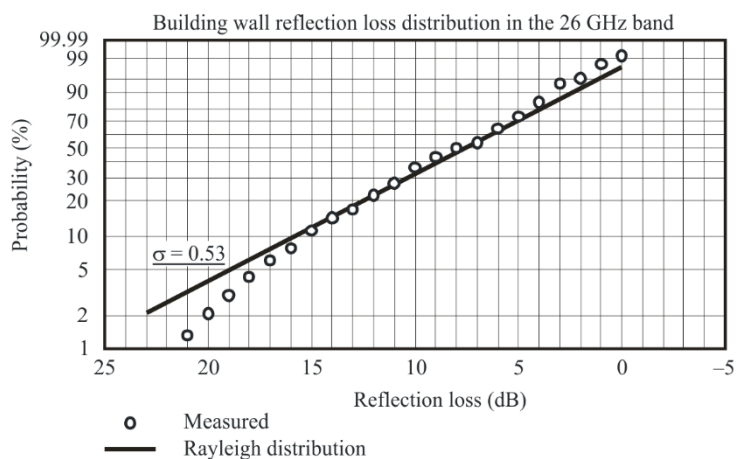
5   Interference

Cellular radio systems are designed such that there is a trade-off between the frequency reuse pattern and the carrier to interference ratio, *C/I*. A minimum *C/I* might be necessary for a certain system to operate satisfactory, i.e. according to specified performance.

Given the minimum *C/I* required it becomes easy to issue a regular frequency reuse pattern that satisfies the requirement. However, terrain features should be taken into account and the suitable base station location should be selected with care to achieve the wanted performance of the radio access system.

In most cases, only a few users will be affected due to their narrow beam terminal antennas. The beamwidths are of the order of 2 to 3 degrees. For users that can be affected, the models in Recommendation ITU-R P.452 and ITU-R P.530 can be used to estimate the percentage of time that harmful non-LoS and LoS enhanced signals, respectively, arise from the interfering base station. However, no data are available above 37 GHz to support the predicted values.

An assessment of the problem of interference was made by using the data from 111 locations studied in an area coverage measurement campaign in the United Kingdom. A second transmitter was considered as a potential interference source. In the whole dataset, only one position showed a signal from the unwanted transmitter above the noise threshold within the beamwidth of the antenna pointed at the wanted transmitter, and even then, the wanted to unwanted signal ratio was found to be 15 dB. This would seem to confirm the fact that inter-cell interference is likely to be of little significance due to the narrow beamwidth of the receiver antennas.